

# EMPIOT: An Energy Measurement Platform for Wireless IoT Devices

Behnam Dezfooli\*, Immanuel Amirtharaj†, and Chia-Chi Li‡

Internet of Things Research Lab, Department of Computer Engineering, Santa Clara University, USA  
Email: \*bdezfooli@scu.edu, †iamirtharaj@scu.edu, ‡cli1@scu.edu

**Abstract**—Profiling and minimizing the energy consumption of IoT devices is an essential step towards employing IoT in various application domains. In this paper we propose EMPIOT, an accurate, low-cost, easy to build, and flexible, power measurement platform. We present the hardware and software components of this platform, and study the effect of various design parameters on accuracy. In particular, we analyze the effect of driver, bus speed, input voltage, and buffering mechanism, on sampling rate, measurement accuracy and processing demand. These extensive experimental studies enable us to configure the system in order to achieve its highest performance. We also propose a novel calibration technique and report the calibration parameters under various settings. Using five different IoT devices performing four types of workloads, we evaluate the performance of EMPIOT against the ground truth obtained from high-accuracy devices. Our results show that, for very low-power devices that utilize 802.15.4 wireless standard, measurement error is less than 4%. In addition, for 802.11-based devices that generate short and high power spikes, error is less than 3%.

**Index Terms**—Energy Efficiency, Testbed, Accuracy, Linux, I2C Driver, 802.15.4, 802.11.

## I. INTRODUCTION

THE importance of low-cost and accurate energy measurement of IoT devices is justified from two important aspects: First, the percentage of energy consumed by connected devices is being increased due to the significant growth in the number of IoT devices. Gartner predicts the number IoT connected devices surpasses 20 billion by 2020 [1]. Second, IoT devices are mostly battery-powered or rely on energy harvesting. Therefore, it is important to measure and reduce the power consumption of these devices to satisfy the QoS requirements of applications.

Analytical and simulation-based energy estimation tools multiply the time spent in each state (e.g., sleep, processing, transmission/reception) by the power consumed in that state. This approach, however, is not accurate due to the complexities of identifying power consumption in each state [2]–[6]. Firstly, the energy consumption of all the operational modes may not be

available for a given system-on-chip (SoC). For example, the datasheet may include only the average current consumption for nominal transmission power values. As another example, the energy consumption of the processor depends on its utilization level, frequency scaling, and I/O operations [7]. Secondly, IoT boards usually include a SoC and several peripheral components (e.g., ADC, sensors, memory). Therefore, even if the energy characteristics of the SoC are known, estimating the total energy consumption of the board is very challenging. Thirdly, code structure, algorithms, and data structures affect the energy consumption of the IoT system. For example, when a cache memory is present, the type of the data structures used affects cache performance when memory allocation is contiguous. Finally, it is difficult to simulate and evaluate the properties of real-world environments (e.g., interference) and study their effects on energy consumption [8]–[10]. Despite these shortcomings, most of the research contributions on low-power wireless IoT systems rely on simulation due to its simplicity.

Although the commercial energy measurement platforms provide very high accuracy, they are costly and bulky. For example, Keysight 34465A costs more than \$1300 with 2MB storage and maximum sampling rate 50Ksps. Similarly, Keithley 7510 [11] costs more than \$3500 with 2MB storage and sampling rate up to 1Msps. In addition, due to their size and cost, these devices are not viable solutions to monitor the energy consumption of a large number of IoT devices in a testbed. Furthermore, their programmability is very limited and inflexible. These shortcomings also apply to the Monsoon power meter [12] (which costs more than \$800), a widely-used platform by academia [13], [14].

Due to these challenges, the research community has proposed several power measurement platforms. Based on their main shortcoming, these platforms are classified into the following categories: (i) *complex* (e.g., [4], [7], [15]–[18]), (ii) *limited supported range* (e.g., [5], [15], [19]–[23]), and (iii) *low accuracy* (e.g., [3], [24]). The platforms of the first category present a complex circuitry, which makes the device costly and hard to build. For the second category, the power measurement platforms cannot be

used with a wide variety of IoT devices due to their limited current measurement range, which is a few tens of millamps. Specifically, the new generation of IoT devices utilize wireless technologies (such as 802.11) that result in current spikes as high as 700mA. Finally, if the accuracy of an energy measurement platform is low, then it cannot be used for effective study, development and debugging of IoT devices. In addition to these shortcomings, most of these platforms ignore the effect of voltage variation on energy measurement [4], [5], [17], [19]. Furthermore, in terms of accuracy analysis, evaluations are very limited and mostly include only one IoT device type [4], [15]–[17].

In this paper we introduce EMPIOT, an accurate, low-cost, easy to build, and flexible, power measurement platform. EMPIOT has two main components: a shield board, which includes a low-cost INA219 [25] energy monitoring chip, and a base board, which runs the controlling and data collection software. The shield board performs both current and voltage measurement and its cost is less than \$5. Depending on the configuration used, INA219 can measure currents and voltages as high as 3.2A and 32V, respectively. The software, written in C++, is composed of two threads for communication with the shield as well as computing energy and saving the data to a file. Despite the simplicity of its hardware, in this paper we show the effect of various design parameters on performance through extensive experimental studies. Specifically, we use two I2C drivers, namely BCM [26] and Linux driver [27], and show that the BCM driver achieves higher speed, lower energy consumption, and predictable timing characteristics. We also evaluate the effect of input voltage on sampling rate and measurement accuracy. Our results show that, reducing the shield’s operational voltage increases conversion time and lowers sampling rate. In addition, we confirm that this platform can run on variable power sources without affecting accuracy. In fact, the accuracy of current and voltage measurement are always within  $100\mu\text{A}$  and 4mV, respectively. We also study the effect of batched and continuous file writes, as well as driver, on the energy consumption of the base board. We show that the BCM driver and batched write operations considerably reduce the energy consumption.

In order to calibrate the platform, we have designed a *programmable calibration tool* (PCT), which enables us to generate currents and voltages in a wide range and precisely control the duration of each change. Using PCT, we calibrate EMPIOT for currents up to 800mA. We study the accuracy of this platform through using five different IoT devices and four types of loads. Our results confirm that measurement error is less than 4% for very low-power devices that use the 802.15.4 wireless standard and generate peak current 30mA. In addition, the error is less than 3% for 802.11 devices that their cur-

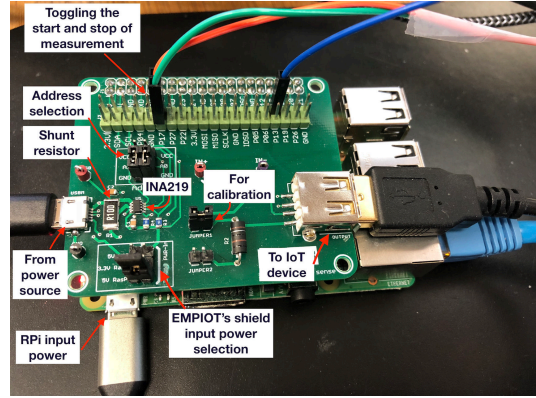


Fig. 1: Components of EMPIOT.

rent consumption surpasses 100mA. We also show that neglecting voltage variations in the energy measurement process may result in up to 0.5% increase in measurement error, especially for battery-powered 802.11-based IoT devices.

We emphasize that this paper does not intend to propose a complex power measurement tool. Rather, we study if and how the EMPIOT shield, or even an existing off-the-shelf INA219 breakout board (such as [28]), can be used for accurate power measurement of a wide variety of IoT devices.

The rest of this paper is organized as follows: Section II presents the platform components and studies the effect of various parameters on design. The calibration methodology and results are presented in Section III. Section IV studies the accuracy of EMPIOT. We study related work in Section V. We conclude the paper in Section VI.

## II. PLATFORM DESIGN

In this section we present the hardware and software design of EMPIOT. We also study the implications of design choices on performance through extensive empirical evaluations.

### A. Hardware

EMPIOT is composed of a shield that is installed on and communicates with a Raspberry Pi (RPi). This is demonstrated in Figure 1. The core of the shield is an INA219 [25], which is a low-cost (~\$2) current and bus voltage monitoring chip. INA219 is available in two flavors, INA219A and INA219B. We use INA219B due to its lower (0.5%) variations versus temperature. The energy draw of the chip is 1mA, and it can operate using a 3 to 5.5V supply. INA219 measures bus voltage directly, and current is measured through digitizing the voltage across a shunt resistor.

The ADC's basic resolution is 12 bits, and 1 LSB step size for shunt voltage and bus voltage are  $10\mu\text{V}$  and  $4\text{mV}$ , respectively. The ADC is a delta-sigma type and uses high frequency (500KHz) to collect analog samples. After collecting samples, the delta-sigma ADC uses a low-pass digital filter for noise reduction, and a decimator averages the analog samples. The INA219 datasheet mentions that the duration of these operations for 12 and 9-bit sampling resolutions are  $532\text{-}586\mu\text{s}$ , and  $84\text{-}93\mu\text{s}$ , respectively. However, as we will show in Section II-C1, the actual sample preparation time is longer than these reported values.

The full scale voltage range supported across the shunt resistor is 40mV. Therefore, as the ADC resolution is 12 bits, one LSB size for shunt voltage is  $40/(2^{12} - 1) = 9.768\mu\text{V}$ . We have used a  $0.1\Omega$  shunt resistor with 0.5% accuracy. Therefore, EMPIOT's current resolution is  $100\mu\text{A}$  for currents up to 400mA. Depending on the maximum possible current, the power gain amplifier (PGA) can be configured to achieve the full-scale range through dividing shunt voltage by 2, 4, or 8. Therefore, shunt voltage in four various ranges can be measured:  $[0, 40]\text{mV}$ ,  $[0, 80]\text{mV}$ ,  $[0, 160]\text{mV}$ ,  $[0, 320]\text{mV}$ . The maximum supported bus voltage is either 16V or 32V, depending on the configuration applied. When configured for 16V, the accuracy of bus voltage measurement is  $16/(2^{12} - 1) = 3.907\text{mV}$ . Considering the nominal operational range of IoT devices, in this paper we assume current and voltage are less than 800mA and 5.5V, respectively.

INA219 supports I2C communication, where the minimum and maximum bus speeds are 0.1MHz and 2.5MHz, respectively. We chose RPi as the underlying platform to configure the chip and collect the results because: (i) its I2C rate is fast enough to support the sample generation rate of INA219, (ii) the memory card enables power sampling for very long durations, (iii) it can be used for serial communication with, remote reprogramming, and debugging of the attached IoT device, (iv) existence of multiple communication technologies (Ethernet, WiFi) simplify testbed setup and remote access.

### B. Software

The pseudo-code of the software is given in Algorithm 1. At a high level, the program consists of the `main` function and two threads. The `main` function first initializes the I2C driver and configures the bus speed. The two drivers we used for this work are BCM [26] and Linux i2c-dev [27] (version 4.4). In the rest of this paper we refer to these drivers simply as *BCM* and *Linux*. Next, INA219's configuration registers are programmed to adjust gain and resolution. The programmed gain value determines the maximum measurable current, and resolution refers to the number of bits per sample. The `main` function then initiates two threads: the `sampler` thread polls the

conversion ready bit of the chip, and when set, it reads the bus voltage and shunt voltage values. In addition, the current system time (in nanosecond) is read using the `clock_gettime()` system call. As this system call is used to add timing information to each sample, it is important to ensure its delay is negligible. To this end, we used a high sampling rate (500MHz) logic analyzer, and we observed that pin toggling delay using BCM library is 40ns. Then, we toggled the pin right before and after the system call. This study showed that the delay of this system call is around 445ns with negligible variations; therefore, this provides a reliable mechanism to append a time stamp to each sample collected, which is required for energy calculation.

The `sampler` thread also computes energy consumption through calling the `compute_energy()` function, which implements the Riemann integral approach. In addition to energy calculation, raw data are written to a file. To this end, we introduced thread `sample_writer` to read data off a buffer and write to a file. We employed two buffering mechanisms to implement *batched* and *continuous* file write operations: When using *two buffers*, the `sampler` thread and `sample_writer` thread use two different buffers. When a buffer is full, the `sampler` thread unblocks the `sample_writer` to flush that buffer, thereby entries are batched and then written to the file. Meanwhile, the `sampler` thread uses the other buffer. The other approach is using a single *circular buffer*. In this approach, as soon as a new entry is written to the buffer, the `sampler` thread signals the `sample_writer` thread to write that entry to the file. In this case, a mutex locks the buffer to avoid concurrent accesses. For both cases the buffers are implemented as fixed-size arrays allocated on stack memory to avoid the overhead of memory re-allocation. This also results in better utilization of cache memory due to the contiguous placement of array entries in random access memory.

The software supports raw data collection and energy measurement: (i) for a given time duration, (ii) after a certain number of samples were collected, and (iii) by receiving an external trigger to indicate the start and stop of measurement. For the trigger case, falling and rising edge interrupts trigger the start and stop of measurement. Using this feature, one can annotate an IoT device's code to start and stop the measurement at particular locations; thereby providing fine-grained energy measurement of various operations such as encryption and transmission.

### C. Design Parameters

In this section we study the effect of various design parameters on performance in terms of sampling rate, sampling offset, accuracy, and energy consumption of the base board.

**Algorithm 1:** EMPIOT’s Software

```

1 function main()
2     setup the I2C driver (BCM/Linux) and bus speed;
3     configure the INA219 gain and resolution;
4     create thread sampler;
5     create thread sample_writer;
6     return;
7 thread sampler()
8     while sampling is enabled do
9         while conversion ready == 0 do
10            check the bit;
11            read bus voltage and shunt voltage values;
12            compute_energy(prev_smp, new_smp);
13            if use two buffers then
14                if use_buffer1 == true then
15                    add entry to buffer1;
16                    if buffer1 is full then
17                        signal the sample_writer thread;
18                    use_buffer1 == false;
19                else
20                    add entry to the buffer2;
21                    if buffer2 is full then
22                        signal the sample_writer thread;
23                    use_buffer1 == true;
24            else if use a circular buffer then
25                lock the buffer;
26                add entry to the buffer;
27                unlock the buffer;
28                signal the sample_writer thread;
29 thread sample_writer()
30     if use two buffers then
31         if use_buffer1 == true then
32             flush buffer1 to the file;
33         else
34             flush buffer2 to the file;
35     else if use a circular buffer then
36         lock the buffer;
37         write entry to the file;
38         unlock the buffer;
39 function compute_energy(prev_smp, new_smp)
40     prv_power = (prv_smp.voltage) × (prv_smp.current);
41     new_power = (new_smp.voltage) × (new_smp.current);
42     time_diff = (new_smp.time) × (prv_smp.time);
43     new_energy = new_power × time_diff ;
44     tri = (new_power - prv_power) × time_diff / 2 ;
45     new_energy -= tri;
46     energy += new_energy;

```

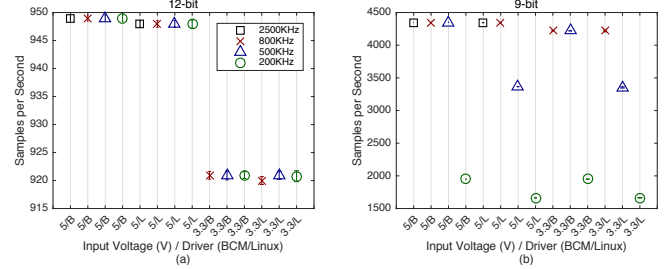


Fig. 2: Sampling rate for (a) 12-bit resolution and (b) 9-bit resolution. Error bars show 95% confidence interval.

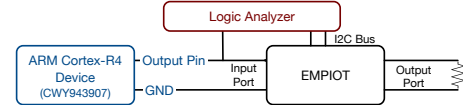


Fig. 3: In order to measure I2C read delay, the logic analyzer captures I2C communications. To measure sampling delay offset, the logic analyzer captures both "Output Pin" status and I2C communications.

more details as follows.

In order to evaluate software overhead, we measured the time spent by the **sampler** thread between collecting a sample and the next polling of conversion ready bit. Using a high-speed logic analyzer, our results show that the processing overhead of the **sampler** thread is  $0.46\mu\text{s}$ , which is negligible. To measure *I2C read delay*, we used a simple code that continuously reads two bytes from the EMPIOT’s shield board. After capturing I2C traffic by a logic analyzer we compute the interval between sending I2C addresses. Figure 4 shows the results<sup>1</sup>. This figure reveals the effect of bus speed and driver on read delay. In particular, the BCM driver achieves a faster and more stable I2C performance compared to Linux driver. In fact, for a given baud rate, Linux I2C read is at least  $20\mu\text{s}$  slower than BCM. In order to justify the lower performance of Linux driver compared to BCM, we used **strace** [29] to capture the system calls made by the software. Our evaluations show that when using BCM, the number of system calls is always fixed (exactly 181) and does not depend on the sampling rate. We also observed that these system calls are only made during the initialization of the BCM driver, after which the software directly communicates with the driver. In contrast, when using the Linux driver, all the I2C communication requests pass through the kernel; therefore, the number of system calls depends on the sampling rate. Figure 4 also shows that the I2C delay of Linux driver has higher variations compared to BCM: the average range of

1) *Effect of input voltage, driver, and bus speed, on sampling rate:* Figure 2 shows sampling rate versus bus speed, driver, and input voltage, where "input voltage" refers to the power source of INA219 on EMPIOT’s shield. The main observations are as follows: First, the sampling rate is lower than the conversion rate supported by the chip. For example, for 12-bit conversion, the sampling rate is lower than the 1.8KHz ADC conversion rate reported in the INA219 datasheet. Second, a lower voltage results in a lower sampling rate. Third, reducing the bus speed to as low as 200KHz results in sampling rate reduction. Fourth, the Linux driver affects sampling rate for 9-bit resolution. We study these observations in

<sup>1</sup>Please note that we did not report the results for bus speed 2500KHz and input voltage 3.3V because we observed a very unreliable I2C communication in this condition. We believe that INA219 cannot keep up with this high clock rate when the voltage is 3.3V

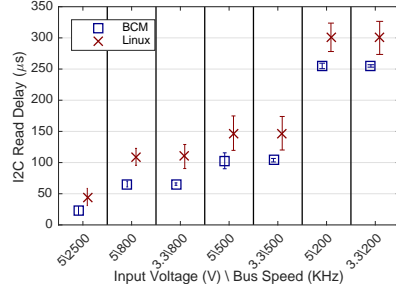


Fig. 4: I2C read delay measured as the time interval between issuing a read command and reception of requested bytes. Error bars show 95% confidence interval.

variations for Linux I2C read delay is  $22\mu\text{s}$ , and for BCM this value is  $4\mu\text{s}$ . These results indicate that the Linux driver does not achieve a reliable rate communication with mission-critical and high rate sensors, such as those used in medical and industrial applications. The effect is also obvious when using 9-bit sampling (cf. Figure 2(b)). For example, when using 500KHz bus speed, using the Linux driver reduces sampling rate to 3360, compared to the 4350 samples collected per second when the BCM driver is in use. From the software point of view, the overhead of Linux driver affects the number of times the conversion ready bit is polled per sample collection round. Table I reports the results. Therefore, the Linux driver falls behind the sample conversion rate when the sampling rate is high.

We next analyzed the time interval between a change in input and reading the corresponding value, which is referred to as *sampling offset*. In order to identify the causes of sampling offset, we used the experiment shown in Figure 3. To introduce a quick and predictable change in power, we have used a pin toggle using an ARM-Cortex R4 board (CWY9443907 [30]) which sets a pin from high to low (i.e., 3.3V to 0V) in 50ns. For this experiment, the "Output Pin" in Figure 3 is initially high (3.3V). At particular intervals, the pin is set to low (0V) and remains in this state for 2ms. We compute sampling delay offset through measuring the interval between setting a pin to low and collecting the corresponding sample. To this end, a logic analyzer logs the status of "Output Pin" as well as I2C communications. Figure 5 shows the measured values. Since I2C read delay is independent of input voltage (as Figure 4 shows), the results of Figure 5 indicate longer conversion time when using a lower voltage value, i.e., 3.3V. For example, increasing conversion time by  $64\mu\text{s}$  decreases the number of samples collected per second by 47. As the power measurement chip uses a delta-sigma ADC, we believe that the lower voltage value slows down the operation of the decimator and averaging circuitry.

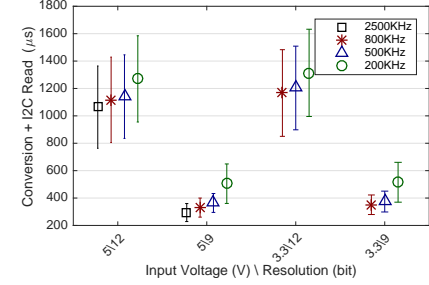


Fig. 5: Sampling offset, which reflects the interval between a change in input current and reading the corresponding value. We used BCM driver for this experiment. Error bars show 95% confidence interval.

TABLE I: Polling rate of conversion ready bit using BCM and Linux drivers for 12 and 9-bit resolution.

		Polling Rate			
		2500KHz	800KHz	500KHz	200KHz
12-bit	BCM	45	15	9	3
	Linux	23	9	6	2
9-bit	BCM	9	2	1	1
	Linux	4	1	1	1

## 2) Effect of Input Voltage on Measurement Accuracy:

In this section we analyze the effect of input voltage variations on accuracy. We consider the following voltage sources to run the INA219 of EMPIOT's shield board:

- External ( $x\text{VExt}$ ): A  $x\text{V}$  external DC power supply [31].
- 5V from RPi (5VRPi): The 5V pin of RPi header.
- 5V from RPi with a load (5VRPi w/Load): The 5V pin of RPi header. In addition, the RPi's USB port is connected to a Cypress CYW943907 IoT device that its idle energy consumption is about 100mA, but periodically wakes up and sends ping packets that result in up to 400mA current consumption.
- 3.3V from RPi (3.3VRPi): The 3.3V pin of RPi header.

We have used an industrial-grade DMM [11] with sampling rate 500Ksps to measure the variations of these power sources. The %95 variations of these sources are as follows: 5VExt: 2mV, 5VRPi: 103mV, 5VRPi w/Load: 300mV, 3.3VRPi: 24mV. Caused by operating system processes and EMPIOT software, we observe that RPi as a power source exhibits higher variations compared to 5VExt. Nevertheless, in order to simplify the design and reduce its cost, we are interested to confirm if RPi can be used as the source of power for EMPIOT's shield board.

In order to measure accuracy across a wide range, we used three different fixed loads: 200 $\mu\text{A}$ , 5mA and 100mA. These loads are generated by connecting the shield's output to three different resistors. Figure 6 presents the effect of voltage variation on the accuracy of bus voltage and current measurement. These results show the variability of measurements caused by factors such as

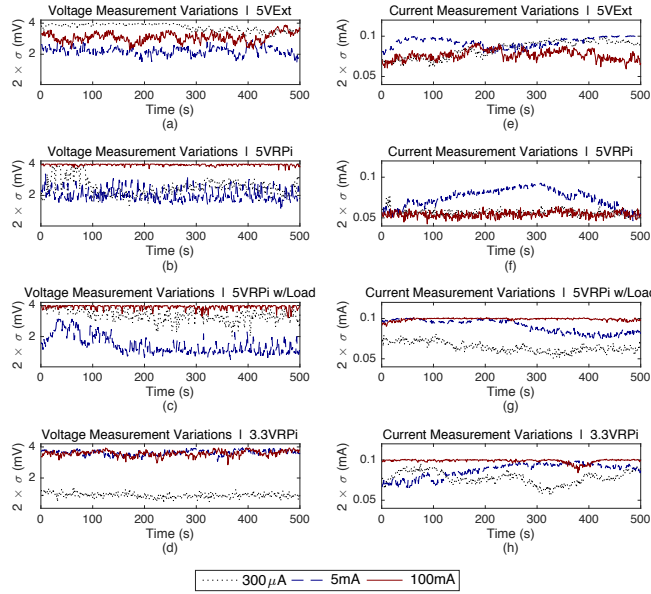


Fig. 6: The measurement variations of voltage (sub-figure (a) through (d)) and current (sub-figure (e) through (h)) over time for three different loads and various input sources. Sampling resolution is 12 bit. The y-axis is the 95% range of variations.

electromagnetic interference and white noise. However, the important observation is that, irrespective to the source of power and load value, the measurement error of EMPIOT is always less than 4mV and 0.1mA for bus voltage and current, respectively. The reported error ranges comply with the values we previously mentioned for INA219 (cf. Section II-A).

*3) Effect of buffering mechanism, driver, and sampling rate, on energy consumption:* In this section we investigate the energy consumption of the RPi running EMPIOT’s software. To this end, we have used two EMPIOT boards, where a board measures the energy consumption of another board. In addition to energy, we have logged the time of writing each sample to the file through toggling a pin and logging pin activation times. This technique avoids introducing extra software overhead to log file write activities. To remove the variations caused by Ethernet communication, we used UART port to communicate with the RPi board whose energy is being measured. When using UART instead of Ethernet, in addition to reducing power variations, the energy consumption of the RPi is reduced by about 30mA.

Figure 7 shows the results. Blue bars indicate file write activities. As it can be observed, using the circular buffer mechanism results in continuously writing to the flash memory, which in turn increases the energy consumption. For example, for 9-bit resolution and BCM driver, the base power of the RPi is increased from 1.25W to 1.3W when using the circular buffer mechanism (compare sub-

figure (a) and (c)). In this case, the circular buffer increases the activity time of the `sample_writer` thread and increases processor utilization by about 15%. Since the `sample_writer`’s processor core utilization is around 98%, this increase requires the utilization of another processor core, thereby preventing core sleep.

Figure 7 also reflects the higher energy consumption of the Linux I2C driver. For example, when using 12-bit resolution, using the Linux driver increases the base power to 1.38W, compared to 1.26W achieved with the BCM driver (compare sub-figure (e) and (f)). As we discussed earlier, I2C communication through the Linux driver results in a significantly higher number of system calls, which increases processing load.

In this paper we used a RPi3 board as the EMPIOT’s based board. However, when Ethernet port and high processing power are not required, cheaper and more power-efficient boards such as Raspberry Pi Zero with Wi-Fi (RPiZW) can be employed. Our studies show that for a RPiZW with an active Wi-Fi connection, using the BCM driver and batched write operations results in 670mW power consumption. Using the circular buffer and Linux driver increases power consumption to 718mW and 685mW, respectively.

Although we have used a small buffer size (5000) for these experiments to reveal the effect of batched write operations, a much larger buffer size results in a higher energy saving. In our implementation, each sample entry is 16 bytes: 8 bytes to store `timespec`, 4 bytes for bus voltage, and 4 bytes for current. Even if only 30% of the 1 GB RAM of RPi3 or 25% of the 512MB of RPiZW is used, then the number of entries kept in random access memory before each file write will be 19,660,000 and 8,388,608, respectively. This shows that batching can be easily used to minimize energy consumption.

### III. CALIBRATION

Calibration is an essential part of the design. Factors such as the resistance of the shunt resistor path, inaccuracy of shunt resistor, and ADC non-linearity, cause difference between EMPIOT’s measurements and a ground truth.

In order to perform current calibration, we need a load that can generate currents within the supported measurement range of EMPIOT. Although current variations can be generated through using an IoT device, this method does not result in an accurate calibration due to the following reasons: First, the duration of a change in current draw may not be long enough to match the samples collected. In other words, due to the fast variations of current as well as the difference in the sampling offset of the DMM and EMPIOT, correlation of the samples collected by the two devices is very challenging. For example, when the current draw changes suddenly,

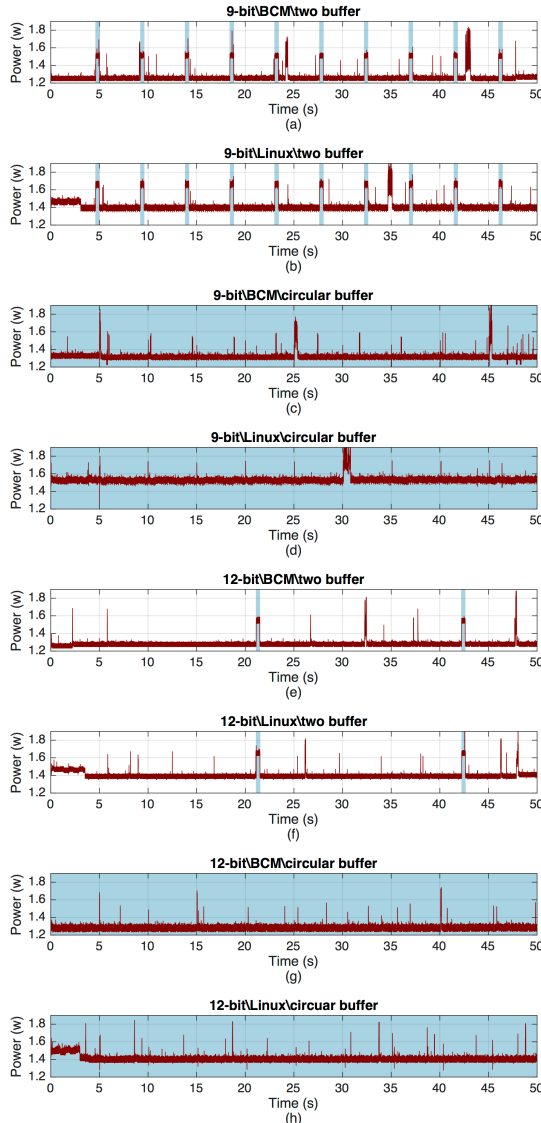


Fig. 7: The effect of sampling resolution, driver, and buffering mechanisms, on the energy consumption of the RPi running EMPIOT software.

some values may not be captured by EMPIOT due to its lower sampling rate compared with a DMM. Furthermore, DMM and EMPIOT might report the variations with different time offsets. Therefore, subtracting the pairwise values does not reflect a realistic measurement error. If the error of EMPIOT versus DMM is in fact a linear function, then the aforementioned calibration errors may prevent us to find a linear fit or cause a linear function that its slope is higher or lower than the real value. In addition, the IoT board may not cover the supported current range of EMPIOT, which results in calibration gaps. In fact, turning on each component (such as RF transceiver) results in a jump in energy

consumption, and it is almost impossible to generate a linear increase. Another solution is to use a potentiometer as the load. However, similar to using an IoT device, as we cannot predict the transition and duration of drawing a particular current value, the measurement offsets affect calibration error. Furthermore, potentiometers usually support low current values, and calibration for currents higher than 100mA requires an expensive potentiometer. Due to these limitations, the existing works perform calibration either: (i) manually by using fixed resistor values [5], [16], [19], or (ii) by using expensive equipment [18], [22], [32].

In order to create a scalable platform infrastructure for ADC calibration, we have designed a low-cost, accurate and *programmable calibration tool*, named PCT, which provides dynamic voltage and current ranges. PCT is in fact a programmable load that its resistance and timing characteristics are controllable. PCT is configured by a software (written in Python) running on a RPi. This software controls reconfiguration frequency and records output settle time between two consecutive configurations. Specifically, if reconfiguration frequency is  $t$ , the PCT software records the output settle times at  $n \times t + t/2$ , where  $n = \{0, 1, 2, \dots\}$  corresponding to all the supported output values. Recording output settle instances enables us to correlate the measurement values of DMM and EMPIOT when the load is stable. Furthermore, this feature prevents the need for accurate time synchronization of DMM and EMPIOT.

One of the key advantages of PCT is its large dynamic output range for both current and voltage. By using a high-accuracy digital potentiometer and well-calculated resistor combinations, the output range of PCT spans between 0.5mA to 1A for current and 0.06mV to 5.5V for voltage. We use 256-position 10k digital potentiometer AD5200 [33] as the base block, and connect it in parallel with multiple resistor paths. These resistors are attached to a switch network implemented by four ADG1612 [34], each including quad SPST switches. Since the digital potentiometer cannot handle currents higher than 20mA, our design supports high current ranges by switching on/off resistor paths. Specifically, a new resistor path is enabled whenever a 20mA or a 100mA increase in current is required, and the digital potentiometer is used to fine-tune current in range 0-20mA. By programming the resistance value, PCT can generate various current and voltage values. The PCT software programs AD5200 and ADG1612 through SPI interface and GPIOs. The entire solution costs about \$100, including manufacturing costs. This is less than 1% of the cost compared to current commercial solutions.

PCT generates line interrupts to trigger the start and stop of measurements by EMPIOT and DMM. As mentioned earlier, EMPIOT supports measurement start

and stop through line interrupts. To trigger the DMM, we have used a high-accuracy and programmable device [11] that exposes several programmable GPIO pins. We have developed a Python script using SCPI (Standard Commands for Programmable Instruments) to configure the sampling rate and enable the DMM to start and stop sampling based on the line interrupts received. This script communicates with the DMM through a TCP/IP connection and transfers the sampled data from the DMM buffer to a PC when a measurement completes.

EMPIOT's shield includes a jumper to enable current flow from input to output (cf. Figure 1). For calibration purposes we have removed this jumper and connected the pins to a DMM; thereby, EMPIOT and DMM measure current simultaneously. Instead of pairwise comparison of the traces collected by EMPIOT and DMM, we use the timing data logged by the programmable load. As the timing data reflects load stability instances, we can safely compare the two closest entries of the traces collected by DMM and EMPIOT.

One of the goals of this paper is to show if an off-the-shelf INA219 breakout board can be used instead of EMPIOT's shield with the software and configuration parameters proposed in this work to achieve a high level of accuracy. To this end, in addition to reporting calibration data for EMPIOT's shield, we have used an INA219 breakout board [28] to study the effect of hardware design on calibration. This breakout board has been installed on a bread board and communicates with a RPi running EMPIOT's software. Figure 8 shows the measurement errors of three EMPIOT boards and three breakout boards conducted in a normal indoor temperature 25°C. Please note that the left value above each figure refers to the maximum supported current configured through the programmable gain amplifier (PGA). As it can be observed, EMPIOT's shield presents lower error compared to the breakout boards. Since INA219 measures current through a shunt resistor, the distance and impedance of the circuit path between the resistor and chip highly affect measurement accuracy. Therefore, the higher accuracy of EMPIOT's shield is due to the ticker and shorter path used. In terms of input voltage, using 5V instead of 3.3V slightly reduces error. In addition, Figure 8 shows that the error of EMPIOT's shield increases linearly versus current. However, the breakout boards' error shows a quadratic behavior for currents beyond 300mA. For both these cases, instead of using a calibration table, we simply find the best fitted curves. Table II reports the calibration values for these boards.

In addition to current, the voltage measured may not reflect the actual bus voltage. We used PCT to generate a variable voltage in the range 2V to 5.5V. Our results show that the error of voltage measurement is a fixed offset. In fact, EMPIOT's voltage measurements versus

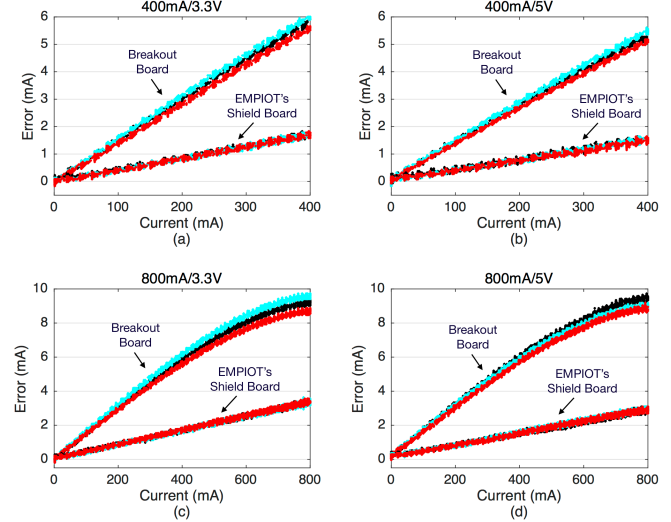


Fig. 8: Current measurement error (mA) versus ground truth. The value above each figure shows the maximum supported current (left side) and input voltage (right side).

TABLE II: Calibration Values

EMPIOT	400mA/3.3V	$I_{empiot} = 0.9957 I_{dmm}$
	400mA/5V	$I_{empiot} = 0.9963 I_{dmm}$
	800mA/3.3V	$I_{empiot} = 0.9949 I_{dmm}$
	800mA/5V	$I_{empiot} = 0.9956 I_{dmm}$
Breakout Board	400mA/3.3V	$I_{break} = 0.9853 I_{dmm}$
	400mA/5V	$I_{break} = 0.9869 I_{dmm}$
	800mA/3.3V	$I_{break} = 0.0079 I_{dmm}^2 + 0.9816 I_{dmm}$
	800mA/5V	$I_{break} = 0.0074 I_{dmm}^2 + 0.982 I_{dmm}$

DMM results in linear function  $V_E = V_{DMM} - 0.027$ . For the breakout board the calibration function is  $V_E = V_{DMM} - 0.097$ .

#### IV. PERFORMANCE EVALUATION

In this section we study the effectiveness of design parameters and calibration on accuracy when EMPIOT's shield and the breakout board are used. Based on the results reported in Section II, the following setting is used for both EMPIOT's shield and the breakout board: (i) BCM driver is used, (ii) bus speed is 2500KHz, (iii) INA219's voltage is 5V, (iv) file writes are batched. Our ground truth is the energy measured by two high accuracy DMMs [11] that record current and voltage with 500Ksps sampling rate and 18-bit resolution. A Python script programs the DMMs in trigger modes. Therefore, when an IoT device begins its operation, EMPIOT as well as the two DMMs start energy measurement. The three main operations performed by the IoT devices are *sleep*, *software encryption* and *transmission*. Please note that transmission includes listening as well due to employing carrier-sense multiple access (CSMA) before each packet send [9]. The encryption operation is used to generate a

high processing load. Depending on the workload used, each node transitions between the available states every 500ms. We introduce three types of loads:

- Workload 1: All the three operations are included,
- Workload 2: Includes send and sleep operations,
- Workload 3: Includes encryption and sleep operations,
- Workload 4: Includes encryption and send operations.

We have used five different IoT boards with various energy characteristics. The first board is a TI SensorTag CC2650 [35]. CC2650 includes an ARM Cortex-M3 processor and supports IEEE 802.15.4 standard. The energy consumption of the board in sleep mode is  $10\mu\text{A}$ , and therefore, we used this board to measure the accuracy of EMPIOT for profiling the energy of very low-power devices. We used TI-RTOS [36] for application development on this device. During the transmission state, the device sends 30-byte 802.15.4 packets as fast as possible. The small packet size introduces quick variations in power consumption.

In order to generate very fast and high temporal variations in power, we used four 802.11-based IoT devices: Avnet BCM4343W [37], Cypress CYW43907 [30], [38], RPiZW, and RPi3. The Avnet board includes an ARM Cortex-M4 processor and supports 802.11a/g/n. When using the power save mode, the minimum energy consumption of the board is around 10mA, processing consumes around 40mA, and packet transmission results in spikes up to 350mA. The Cypress board includes an ARM Cortex-R4 processor and supports 802.11a/g/n. As the board includes other components such as Ethernet chip, the sleep power of the board is around 96mA. The processing power is around 140mA, and packet transmissions increase power consumption up to 400mA. We have used Free-RTOS and WICED Studio [39] for software development on the Avnet and Cypress devices. Furthermore, to generate higher variations in power, the software developed for these devices enable the power save mode (PS-Poll) mechanism so that the radio transitions into sleep mode when it is not transmitting. At certain intervals the radio wakes up and ping packets are transmitted as fast as possible. As ping packets are small, this behavior results in fast and short spikes in power consumption.

For RPiZW, the base and processing power are about 130mA and 180mA, respectively, and 802.11 transmissions result in spikes as high as 300mA. For the regular RPi3, the sleep and processing currents are about 280mA and 330mA, respectively, and 802.11 transmissions increase current consumption up to 500mA. A program (written in c) controls the transition between the three operations provided. Please note that for RPiZW and RPi3 we refer to the process inactivity time as sleep time.

Figure 9 shows the energy consumption of CC2650 and BCM4343W. Although CC2650 shows a clear transition

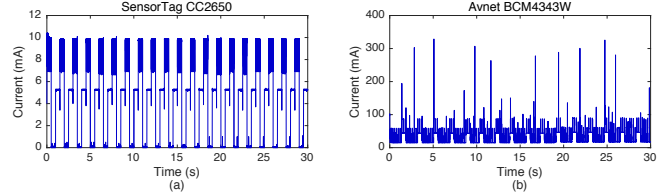


Fig. 9: The energy trace of SensorTag CC2650 and Avnet BCM4343W when transitioning between sleep, encryption and transmission.

between the three states, BCM4343W presents spikes across the trace. It should be noted that in contrast with 802.15.4, 802.11 communication requires association with an access point. Therefore, when 802.11 power save mode is enable, the device wakes up every 100ms to receive the beacon packets generated by the access point.

Figure 10 presents power measurement error when using EMPIOT shield and the breakout board. Error is computed as  $\frac{|E_x - E_{dmm}|}{E_{dmm}} \times 100$ , where  $E$  represents energy.  $E_x$  refers to the energy computed by either EMPIOT or the breakout board. Each marker is the median of 10 experiments, where an experiment is 30 seconds long<sup>2</sup>. These results indicate that EMPIOT is in fact an accurate power measurement platform, even if an off-the-shelf breakout board is used instead of its shield. Comparing sub-figure (a) through (e) shows that energy measurement error is higher when measuring very small currents. Specifically, while the measurement error for 802.11-based boards is less than 2.5%, the error is less than 3.5% for SensorTag. Considering Workload 1 on SensorTag, we observed that more than 40% of variations in current are less than 1mA. However, since the current resolution of INA219 is  $100\mu\text{A}$ , these variations are not captured with a very fine granularity. For example, EMPIOT cannot detect current variations between 3.25mA and 3.27mA because these variations are less than  $100\mu\text{A}$ . Therefore, as the power consumption of SensorTag is significantly lower than that of other boards, small errors in current measurement result in a more considerable effect on total measurement error.

Figure 10 also reveals the effect of calibration on accuracy. In particular, since the measurement error of the breakout board is higher than that of EMPIOT's shield, calibration has a higher effect on accuracy. In addition, this is particularly important for 802.11-based boards because, as Figure 8 shows, the error of breakout board is higher and non-linear for currents higher than 300mA.

Although our studies in Section II-C1 showed that EMPIOT supports around 1000 and 4000 samples per

<sup>2</sup>The 30-second experiment duration is due to the limitation of the DMM used in terms of the number of samples stored in its memory.

second for 12 and 9-bit resolution, respectively, it should be noted that the actual sampling rate of the delta-sigma ADC is about 500KHz, and the decimator averages the analog samples collected per sampling interval. For example, when 12-bit sampling is used for 802.11-based devices, the rapid power variations of these platforms are captured and averaged per millisecond, according to the sampling rate we reported in Section II-C1. Consequently, we observe that EMPIOT achieves high accuracy even in the presence of very fast temporal power variations.

Figure 10 also shows that the measurement error of 9-bit resolution is slightly higher than that of 12-bit resolution. This is particularly obvious for the SensorTag measurements. As we mentioned earlier, compared with the 802.11 devices, SensorTag generates smaller variations in power, thereby a higher resolution is required to capture the changes. Compared with 12-bit, using 9-bit resolution enhances the sampling rate (cf. Figure 2), however, the minimum detectable variation in current is increased to  $780\mu\text{A}$ . For 802.11-based devices with high data transmission rate, the higher sampling rate enables us to capture shorter variations in power. Therefore, the increase in sampling rate compensates the error introduced due to lower resolution.

#### A. Importance of Voltage Measurement

Most of the existing energy measurement platforms ignore the effect of voltage variations on energy measurement (e.g., [4], [5], [17], [19]). To verify the implication of this assumption on accuracy, we have used Workload 1 and computed energy when: (i) the average value of voltage measurements is used, (ii) the voltage samples are used. Error is computed as the difference between these cases. Figure 11 shows the results when a power supply and a battery are used as the sources of power for various types of IoT devices. These results indicate that neglecting voltage would result in up to 0.45% increase in energy measurement error. The impact of voltage on energy measurement depends on various factors including: the stability of power source, the number and intensity of sudden increases in current draw, and the electronic characteristics of the IoT device such as voltage stabilization. For example, when a battery is used, sudden variations of current result in higher measurement error when voltage is ignored. These results also show that the Cypress and Avnet devices cause significant variations in input voltage, compared with RPi3 and RPiZW. Our studies show that these variations are caused by the operations of 802.11 RF transceiver, thereby highlighting the importance of including voltage for 802.11-based IoT devices. On the other hand, the energy consumption of SensorTag and its 802.15.4 radio does not cause any significant variation in voltage.

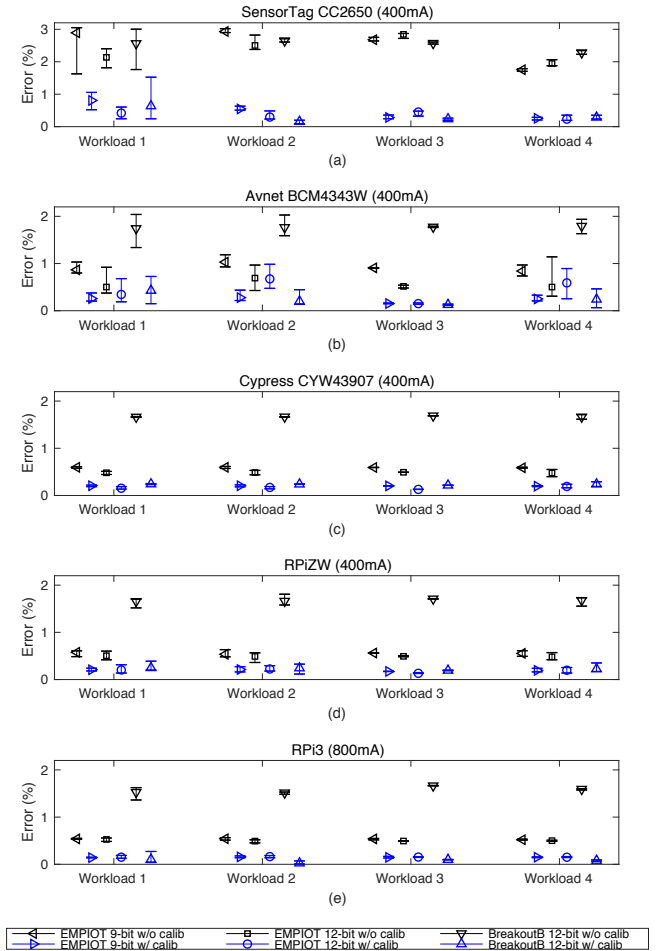


Fig. 10: The energy measurement error of EMPIOT. Error bars show median, lower quartile and higher quartile. Each marker is the median of ten experiments each 30 seconds long.

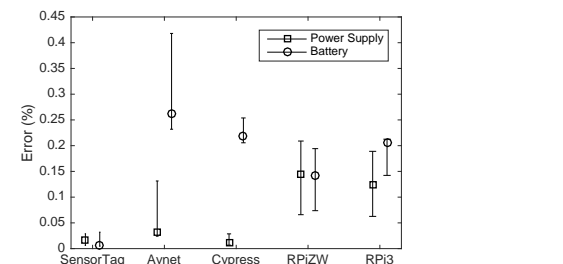


Fig. 11: The effect of ignoring voltage on the accuracy of energy measurement. Error bars show median, lower quartile and higher quartile.

#### B. Discussion

As mentioned earlier, the current measurement resolution of EMPIOT is  $100\mu\text{A}$ . This limitation is problematic when measuring the energy of SensorTag because its sleep current is  $10\mu\text{A}$ . To improve the accuracy of energy measurement, whenever the reported current value is

around  $100\mu\text{A}$ , we simply record value  $10\mu\text{A}$ . However, this mechanism is not applicable to the IoT devices that support multiple low-power modes. For example, EMPIOT cannot capture transitions between  $1\mu\text{A}$ ,  $10\mu\text{A}$  and  $100\mu\text{A}$  low-power states. Since the number of low-power states are usually limited, one solution to overcome this limitation is to explicitly inform EMPIOT about the transition through various mechanisms such as pin toggling or serial communication. In other words, through generating various types of pin activities right before each transition to a low-power mode, EMPIOT is informed to use the value corresponding to that mode.

Another limitation of EMPIOT is its warm-up time. Our studies show that the first 3 to 5 samples collected after initialization are not reliable. Therefore, when using 12-bit resolution, the first 5ms of an operation cannot be measured. This limits the minimum duration of energy measurement. This problem, however, can be simply addressed in software: instead of actually turning on and off the shield board per measurement, we can ignore the samples collected when energy measurement is inactive.

## V. RELATED WORK

In this section we provide an overview of the existing energy measurement platforms. To this end, we classify these works based on their main limitation, as follows.

### A. Costly and Bulky

An oscilloscope is used in [40] to analyze the energy consumption of 802.11 transceivers. Using a current probe is the approach employed in [41] for power monitoring. The current probe relies on the magnetic field generated by current draw; therefore, it cannot be used to detect small currents or variations (milliamps level). The authors in [2] added a shunt resistor to a USB cable and measured both current and bus voltage using USB1608-FSPlus [42], a 16-bit ADC. The USB1608-FSPlus is controlled by a PC and the sampling rate is 1Ksps. All of these approaches are expensive and their size prevents integration with the IoT devices of a testbed.

### B. Complex Circuit

Similar to ICs such as BQ2019 [43], the SPOT [15] platform uses voltage to frequency conversion and relies on the resources of the device under test to operate. In addition, the oscillator and the converter are the sources of noise and error and may interfere with the device under test. More importantly, attaching SPOT to an IoT device is not plug-and-play. SPOT's measurement error is less than 15% and its resolution is  $1\mu\text{A}$ ; however, it assumes the typical operating range of the IoT device is  $5\mu\text{A}$  to  $50\text{mA}$ . LEAP2 [7] is a FPGA-based platform that enables individual monitoring of various components such

as processor and memory. iCount [16] relies on the linear relationship between current and switching frequency of boost switching regulators: counting the switching cycles reflects the current drawn during an interval. A shortcoming of iCount is that it utilizes the resources of device under test and increases its energy consumption. Another limitation of this approach is that boost converters are not always available on IoT boards. For example, both CYW43907 [30] and CC2650 [35] (used in Section IV) utilize internal voltage regulators.

Energy Bucket [17] counts the number of charges and discharges of a buffer capacitor. Although Energy Bucket can measure currents in the range  $1\mu\text{A}$  to  $100\text{mA}$ , the major shortcoming is the dependency of sampling rate on capacitor value. For example, when the current drawn is very small, the inter-sampling interval would be long. In addition, the platform assumes that bus voltage is fixed, and the paper does not include accuracy analysis. Nemo [4] uses a shunt resistor switch composed of a series of resistors. Each resistor is enabled or disabled based on current intensity. The voltage across the resistor switch is amplified using a differential op-amp and then digitized by a 12-bit ADC. Although this technique eliminates the need for a high-precision ADC or an adjustable amplifier, Nemo's processor must quickly react to changes in current and adjust the resistor value. Depending on the input current (which is supported in the range  $1\mu\text{A}$  and  $200\text{mA}$ ) the resolution of Nemo varies in the range  $0.013\mu\text{A}$  to  $48\mu\text{A}$ . Unfortunately, Nemo does not measure bus voltage, and the evaluations are simple and do not include an IoT device with high power variations.

$\mu$ Monitor [18] proposes a power monitor platform based on counting capacitor charging and discharge cycles. For the loads within range  $1\mu\text{W}$  to  $10\text{mW}$ , the accuracy of  $\mu$ Monitor is almost within 10% of the results obtained from a 16-bit ADC that digitizes the voltage value over a shunt resistor. Unfortunately, the evaluations use static loads. Similar to Nemo [4], Potsch et al. [22], [23] propose the use of two shunt resistors ( $1\Omega$  and  $100\Omega$ ) for measuring low and high currents up to  $100\text{mA}$ . Shunt resistor voltages are amplified and then sampled by a 16-bit ADC. A 32-bit microcontroller communicates with the ADC and collects the samples. The actual sampling rate and resolution of this platform have not been evaluated.

In addition to the limitations highlighted, a common shortcoming of the platforms reviewed in this section is their complex circuitry. Specifically, these platforms include various components such as ADC, op-amp, resistor series, high precision capacitors, and processor. Therefore, building these platforms is costly and time consuming. In contrast, EMPIOT is very easy to build, and the cost of a complete platform (shield plus base board) is around \$35 and \$15 when a RPi3 or a RPiZW

is used as the base board, respectively.

### C. Limited Range

PowerBench [19] is capable of providing 5KHz sampling rate and  $30\mu\text{A}$  resolution. PowerBench assumes the maximum current consumption of the host device is 65mA. This platform samples the amplified voltage (51x) across a shunt resistor using a 12-bit ADC. The authors in [5] assume energy profiling requires current measurement only. The error of this platform is less than 5% as long as current is higher than  $20\mu\text{A}$ . However, the maximum supported current is 35mA. iWEEP\_HW [20] employs a multi-layer architecture to measure the power consumption of processor, transceiver, and sensors, using separate ADC channels. This platform uses a PIC18 processor and a 10-bit ADC which measures voltage across shunt resistors. iWEEP\_HW can measure currents up to 40mA with maximum sampling rate 150KHz. PotatoScope [21] is a microcontroller-based oscilloscope that focuses on reliable energy measurement in outdoor environments and in the presence of significant temperature variation. PotatoScope includes an ARM Cortex-M3 processor attached to a 12-bit ADC to sample current and voltage. The voltage across a  $0.47\Omega$  shunt resistor is amplified by 200x. Since the ADC's reference voltage is 2.5V, the maximum measurable current is 26.6mA.

The main shortcoming of these platforms is their limited current measurement range, which is less than 100mA. In this paper we showed that the new generation of IoT devices rely on high data rate technologies that increase temporal power consumption as high as 700mA. Therefore, none of the platforms studied in this section can be used with these IoT devices. The performance evaluation results presented in Section IV confirm the effectiveness of EMPIOT for measuring the energy of 802.11 IoT devices.

### D. Low Accuracy

Energino [3] uses the 10-bit ADC of Arduino boards. The ADC supports input voltage 0 to 5V, therefore, the LSB is 4.88mV and the current measurement resolution is 25mA. Energino uses a Hall-effect current sensor with sensitivity 185mV/A to measure currents up to 5A. The actual sampling rate is 1KHz. NITOS [24] uses the ATmega2560 micro-controller with a 10-bit ADC. Since the Arduino's ADC cannot measure millivolt level variations in voltage, a voltage amplifier has been used. In order to maximize sampling rate, NITOS: (i) uses ADC free running mode, (ii) increases the ADC's prescalar clock from 125KHz to 1MHz, and (iii) uses interrupt service routine to get ADC values. Although these enhancements result in up to 63KHz sampling rate, the accuracy of ADC is reduced by 11% due to the

higher clock used. Furthermore, the current measurement resolution of the platform is 25mA.

## VI. CONCLUSION

The EMPIOT platform presented in this paper enables low-cost, programmable, and accurate energy measurement of a wide range of IoT devices. After explaining the hardware and software components of this platform, we evaluated the effect of various parameters on performance. Our studies show that: (i) the BCM driver results in higher sampling rate and lower energy consumption, (ii) lowering the shield's operational voltage slightly reduces sampling rate, (iii) voltage variations do not affect accuracy, and (iv) using two buffers for batching file writes results in lower energy consumption. In terms of calibration, we developed a programmable load that enables us to generate a wide range of load values and calibrate the platform without requiring precise timing control. We evaluated the performance of EMPIOT using five different IoT devices and four types of workloads. Our results confirm that energy measurement error is less than 3% for IoT devices that utilize 802.15.4 or 802.11 wireless standards. Beyond the scope of this paper, our study on the I2C performance and power efficiency of Linux provides insights into designing Linux-based IoT systems.

## REFERENCES

- [1] Gartner. IoT Units Installed Base by Category (Millions of Units). [Online]. Available: <https://www.gartner.com/newsroom/id/3598917>
- [2] F. Kaup, P. Gottschling, and D. Hausheer, "PowerPi: Measuring and modeling the power consumption of the Raspberry Pi," in *Proceedings of the 39th Annual IEEE Conference on Local Computer Networks (LCN'14)*, 2014, pp. 236–243.
- [3] K. Gomez, R. Riggio, T. Rasheed, D. Miorandi, and F. Granelli, "Energino: a Hardware and Software Solution for Energy Consumption Monitoring," in *Proceedings of the International Workshop on Wireless Network Measurements (WiOpt'12)*, 2012, pp. 311 – 317.
- [4] R. Zhou and G. Xing, "Nemo: A high-fidelity noninvasive power meter system for wireless sensor networks," *Proceedings of the ACM/IEEE International Conference on Information Processing in Sensor Networks (IPSN'13)*, pp. 141–152, 2013.
- [5] T. Trathnigg, M. Jürgen, and R. Weiss, "A low-cost energy measurement setup and improving the accuracy of energy simulators for wireless sensor networks," in *Proceedings of the workshop on Real-world wireless sensor networks*, 2008, pp. 31–35.
- [6] J. Eriksson, F. Österlind, N. Finne, A. Dunkels, N. Tsiftes, and T. Voigt, "Accurate network-scale power profiling for sensor network simulators," in *Proceedings of the International Conference on Embedded Wireless Systems and Networks (EWSN'09)*, vol. 9. Springer, 2009, pp. 312–326.
- [7] T. Stathopoulos, D. McIntire, and W. J. Kaiser, "The energy endoscope: Real-time detailed energy accounting for wireless sensor nodes," *Proceedings of International Conference on Information Processing in Sensor Networks (IPSN'08)*, pp. 383–394, 2008.
- [8] Q. Li, M. Martins, O. Gnawali, and R. Fonseca, "On the effectiveness of energy metering on every node," in *Proceedings of the IEEE International Conference on Distributed Computing in Sensor Systems (DCOSS'13)*, 2013, pp. 231–240.

[9] B. Dezfouli, M. Radi, S. A. Razak, T. Hwee-Pink, and K. A. Bakar, "Modeling low-power wireless communications," *Journal of Network and Computer Applications*, vol. 51, pp. 102–126, 2015.

[10] B. Dezfouli, M. Radi, K. Whitehouse, S. A. Razak, and H.-P. Tan, "Cama: Efficient modeling of the capture effect for low-power wireless networks," *ACM Transactions on Sensor Networks (ToSN)*, vol. 11, no. 1, p. 20, 2014.

[11] Tektronix. DMM7510 7.5-Digit Graphical Sampling Multimeter. [Online]. Available: <https://www.tek.com/tektronix-and-keithley-digital-multimeter/dmm7510>

[12] Monsoon Inc. Monsoon Power Monitor. [Online]. Available: <https://www.msoon.com/LabEquipment/PowerMonitor/>

[13] J. Manweiler and R. Roy Choudhury, "Avoiding the rush hours: Wifi energy management via traffic isolation," in *Proceedings of the 9th international conference on Mobile systems, applications, and services*. ACM, 2011, pp. 253–266.

[14] P. Serrano, A. Garcia-Saavedra, G. Bianchi, A. Banchs, and A. Azcorra, "Per-frame energy consumption in 802.11 devices and its implication on modeling and design," *IEEE/ACM Transactions on Networking (ToN)*, vol. 23, no. 4, pp. 1243–1256, 2015.

[15] X. Jiang, P. Dutta, D. Culler, and I. Stoica, "Micro Power Meter for Energy Monitoring of Wireless Sensor Networks at Scale," *Proceedings of the 6th international conference on Information processing in sensor networks (IPSN'07)*, p. 186, 2007.

[16] P. Dutta, M. Feldmeier, J. Paradiso, and D. Culler, "Energy metering for free: Augmenting switching regulators for real-time monitoring," in *Proceedings of the 7th International Conference on Information Processing in Sensor Networks (IPSN'08)*, 2008, pp. 283–294.

[17] J. Andersen and M. T. Hansen, "Energy Bucket: A Tool for Power Profiling and Debugging of Sensor Nodes," in *Proceedings of Third International Conference on Sensor Technologies and Applications (SENSORCOMM'09)*. IEEE, 2009, pp. 132–138.

[18] S. Naderiparizi, A. N. Parks, F. S. Parizi, and J. R. Smith, "μMonitor: In-situ energy monitoring with microwatt power consumption," in *Proceedings of the IEEE International Conference on RFID (RFID'16)*. IEEE, may 2016, pp. 1–8.

[19] I. Haratcherev, G. Halkes, and T. Parker, "PowerBench: A Scalable Testbed Infrastructure for Benchmarking Power Consumption," in *Proceedings of the International Workshop on Sensor Network Engineering (IWSNE'08)*, 2008, pp. 37–44.

[20] N. Zhu and I. O'Connor, "Energy measurements and evaluations on high data rate and ultra low power wsn node," in *10th IEEE International Conference on Networking, Sensing and Control (ICNSC)*, 2013, pp. 232–236.

[21] R. Hartung, U. Kulau, and L. Wolf, "Distributed energy measurement in WSNs for outdoor applications," *Proceedings of the 13th Annual IEEE International Conference on Sensing, Communication, and Networking (SECON'16)*, 2016.

[22] A. Pötsch, A. Berger, and A. Springer, "Efficient analysis of power consumption behaviour of embedded wireless iot systems," in *Instrumentation and Measurement Technology Conference (I2MTC)*, 2017, pp. 1–6.

[23] A. Pötsch, A. Berger, C. Leitner, and A. Springer, "A power measurement system for accurate energy profiling of embedded wireless systems," in *Proceedings of the 19th IEEE International Conference on Emerging Technologies and Factory Automation (ETFA'14)*, 2014, pp. 1–4.

[24] S. Keranidis, G. Kazdaridis, V. Passas, T. Korakis, I. Koutsopoulos, and L. Tassiulas, "NITOS Energy Monitoring Framework: Real Time Power Monitoring in Experimental Wireless Network Deployments," *SIGMOBILE Mob. Comput. Commun. Rev.*, vol. 18, no. 1, pp. 64–74, 2014.

[25] INA219 Zero-Drift, Bidirectional Current/Power Monitor With I2C Interface. [Online]. Available: <http://www.ti.com/lit/ds/symlink/ina219.pdf>

[26] "C library for Broadcom BCM 2835." [Online]. Available: <http://www.airspayce.com/mikem/bcm2835/>

[27] "Linux I2C Driver." [Online]. Available: <https://www.kernel.org/doc/Documentation/i2c/dev-interface>

[28] "Adafruit INA219 Current Sensor Breakout." [Online]. Available: <https://learn.adafruit.com/adafruit-ina219-current-sensor-breakout/downloads>

[29] strace: Linux syscall tracer. [Online]. Available: <https://strace.io>

[30] Cypress Semiconductor. CYW43907: IEEE 802.11 a/b/g/n SoC with an Embedded Applications Processor. [Online]. Available: <http://www.cypress.com/file/298236/download>

[31] Keysight Technologies. U8000 Series, Single Output DC Power Supplies. [Online]. Available: <https://literature.cdn.keysight.com/litweb/pdf/5989-7182EN.pdf?id=1460471>

[32] R. Lim, F. Ferrari, M. Zimmerling, C. Walser, P. Sommer, and J. Beutel, "FlockLab: A Testbed for Distributed, Synchronized Tracing and Profiling of Wireless Embedded Systems," in *Proceedings of the 12th international conference on Information processing in sensor networks (IPSN'13)*, 2013, p. 153.

[33] Analog Devices. 256-Position and 33-Position Digital Potentiometers. [Online]. Available: [http://www.analog.com/media/en/technical-documentation/data-sheets/AD5200\\_5201.pdf](http://www.analog.com/media/en/technical-documentation/data-sheets/AD5200_5201.pdf)

[34] —. Quad SPST Switches. [Online]. Available: [http://www.analog.com/media/en/technical-documentation/data-sheets/ADG1611\\_1612\\_1613.pdf](http://www.analog.com/media/en/technical-documentation/data-sheets/ADG1611_1612_1613.pdf)

[35] CC2650 SimpleLink Multistandard Wireless MCU. [Online]. Available: <https://www.ti.com/lit/ds/swrs158b/swrs158b.pdf>

[36] TI-RTOS: Real-Time Operating System (RTOS). [Online]. Available: <http://www.ti.com/tool/TI-RTOS>

[37] BCM4343W: 802.11b/g/n WLAN, Bluetooth and BLE SoC Module. [Online]. Available: [https://products.avnet.com/opasdata/d120001/medias/docs/138/AES-BCM4343W-M1-G\\_data\\_sheet\\_v2\\_3.pdf](https://products.avnet.com/opasdata/d120001/medias/docs/138/AES-BCM4343W-M1-G_data_sheet_v2_3.pdf)

[38] Cypress Semiconductor. CYW943907AEVAL1F Evaluation Kit. [Online]. Available: <http://www.cypress.com/documentation/development-kitsboards/cyw943907aeval1f-evaluation-kit>

[39] "WICED: Wireless Internet Connectivity for Embedded Devices)." [Online]. Available: <http://www.cypress.com/products/wiced-software>

[40] L. M. Feeney and M. Nilsson, "Investigating the energy consumption of a wireless network interface in an ad hoc networking environment," in *Twentyith Annual Joint Conference of the IEEE Computer and Communications Societies (INFO-COM'01)*, 2001, pp. 1548–1557.

[41] A. Milenkovic, M. Milenkovic, E. Jovanov, D. Hite, and D. Raskovic, "An environment for runtime power monitoring of wireless sensor network platforms," in *Proceedings of the Thirty-Seventh Southeastern Symposium on System Theory (SSST'05)*, 2005, pp. 406–410.

[42] Measurement Computing Corporation. USB-1608FS-Plus data acquisition device. [Online]. Available: <http://www.mccdaq.com/pdfs/manuals/USB-1608FS-Plus.pdf>

[43] BQ2019: Advanced Battery Monitor. [Online]. Available: <https://www.ti.com/lit/ds/slus465e/slus465e.pdf>